First-principles study of $InVO_4$ under pressure: phase transitions from $CrVO_4$- to $AgMnO_4$-type structure

Sinhué López-Moreno[1],[*,†] Plácida Rodríguez-Hernández[3],[‡] Alfonso Muñoz[3],[‡] and Daniel Errandonea[2¶]

[1]*CONACYT - Centro de Investigación en Corrosión, Universidad Autónoma de Campeche, Av. Héroe de Nacozari 480, Campeche, Campeche 24029, México,* [3]*MALTA Consolider Team, Departamento de Física, Instituto de Materiales y Nanotecnología, and Malta Consolider Team, Universidad de La Laguna, La Laguna 38205, Tenerife, and* [2]*MALTA Consolider Team, Departamento de Física Aplicada-ICMUV, Universitad de Valencia, Edificio de Investigación, c/Dr. Moliner 50, Burjassot, 46100 Valencia, Spain*

E-mail: sinlopez@uacam.mx

[*]To whom correspondence should be addressed
[†]Universidad Autónoma de Campeche
[‡]Malta and Universidad de La Laguna
[¶]MALTA and Universitad de Valencia

Abstract

First-principles calculations have been done to study the $InVO_4$ compound under pressure. In this work, total energy calculations were performed in order to analyze the structural behavior of the experimentally known polymorphs of $InVO_4$: monoclinic α-$MnMoO_4$-type (I), orthorhombic $CrVO_4$-type (III), and the monoclinic wolframite (V). Besides, in this paper we present our results about the stability of this compound beyond the pressures reached by experiments. We propose some new high pressure phases based in the study of 13 possible candidates. The quasiharmonic approximation has been used to calculate the sequence of phase transitions at 300 K: $CrVO_4$-type, III (in parentheses the transition pressure) $\rightarrow$ wolframite, V (4.4 GPa) $\rightarrow$ raspite, VI (28.1 GPa) $\rightarrow$ $AgMnO_4$-type, VII (44 GPa). Equations of state and phonon frequencies as function of pressure have been calculated for the studied phases. In order to determine the stability of each phase we also report the phonon dispersion along the Brillouin zone and the phonon density of states for the most stable polymorphs. Finally, the electronic band structure for the low- and high-pressure phases for the studied polymorphs is presented as well as the pressure evolution of the band gap. Where a change from 3.06 eV at ambient pressure to 1.2 eV at 60 GPa is observed in $InVO_4$, behaving the material as a narrow-gap semiconductor.

1 Introduction

Vanadates AVO_4[1] oxides have been the focus of many studies due to their wide physical properties which leads to important applications in various fields, such as thermophosphorus sensors, high-power lasers, scintillators, active material for gas sensors, catalysis for water splitting and electrolyte for lithium ion batteries, to name a few.[1–10] Several vanadates can crystallize in structures such as zircon,[11,12] scheelite,[13] and monazite,[14] however, to our knowledge, only the vanadates $CrVO_4$-III, $FeVO_4$-II, $TlVO_4$ and $InVO_4$, have been synthesized in the $CrVO_4$-type structure [space group (SG) $Cmcm$, No. 63, $Z = 4$].[6] While

$CrVO_4$-III and $FeVO_4$-II have been studied by using several techniques,[15–19] only the thermodynamic properties,[20] the vibrational spectra,[21] and the photoelectrochemical response[9] were reported for $TlVO_4$. In contrast, there have been more studies dedicated to study $InVO_4$ due to its potential for applications such as a catalyst for production of hydrogen by visible-light driven water splitting.[7–10,22,23]

$InVO_4$ can be synthetized in different polymorphic forms depending on the preparation and temperature condictions: monoclinic α-$MnMoO_4$-type structure $InVO_4$-I (SG: $C2/m$, No. 12, $Z = 8$), $InVO_4$-II (undetermined structure), and orthorhombic $CrVO_4$-type structure $InVO_4$-III (SG: $Cmcm$).[20,24–28] Besides, two high pressure (HP) phases have been reported: $InVO_4$-IV (undetermined structure) and monoclinic wolframite $InVO_4$-V (SG: $P2/c$). Figure 1 (a)-(c) shows the crystal structure of these phases, with the coordination polyhedra for In and V depicted in each figure. The most representative works on this compound have been dedicated to describe the crystalline structure of the phases III and V, whereas there is a latent lack of information regarding phases I, II, and IV, due to their relative stability against to the others. Several studies to determine the ambient conditions structure of the $CrVO_4$-type phase ($InVO_4$-III)[24,25,29] have been reported.

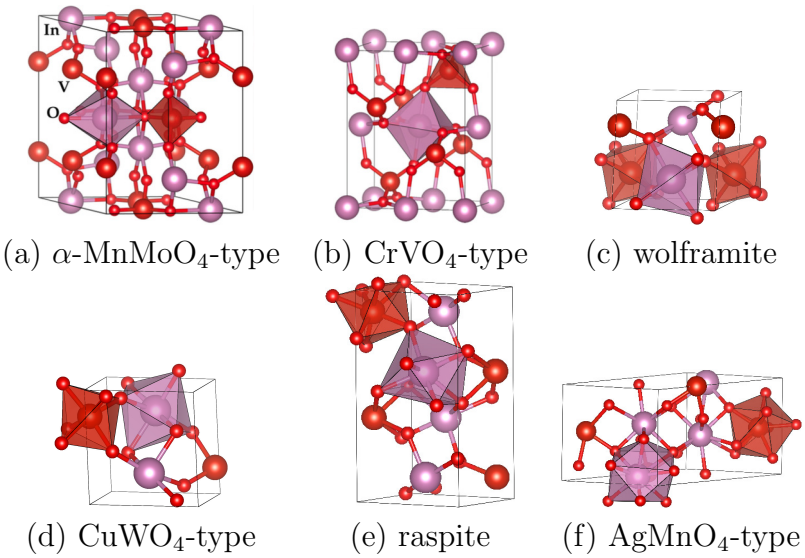

(a) α-$MnMoO_4$-type (b) $CrVO_4$-type (c) wolframite

(d) $CuWO_4$-type (e) raspite (f) $AgMnO_4$-type

Figure 1: Most relevant crystalline structures of $InVO_4$ polymorphs.

Regarding phase V, the wolframite structure matches with the high pressure phase re-

ported for other compounds with $CrVO_4$-type structure such as $InPO_4$ and $TiPO_4$.[30] Besides, this phase is considered as a natural high-pressure post-$CrVO_4$-type structure in the phase diagram proposed for these kind of compounds.[6] Although the study performed by Errandonea *et al.*[25] is a novelty and present important information about the stability of this compound under pressure, other transitions could be observed at higher pressures than those reached in their experiments. Moreover, it has been demonstrated that theoretical studies can provide new insights about the stability of ABX_4 compounds under pressure,[1] which could help to explore and understand the behavior of vanadates beyond the wolframite phase.

As well as studies on the crystalline $CrVO_4$-type structure of $InVO_4$, there have been investigations dedicated to the study of other forms of this compound. In these efforts, it was reported the synthesis and characterization of $InVO_4$ nanotubes arrays.[31–33] It is interesting to mention that these arrays can present either the α-$MnMoO_4$-type structure[31,33] or the orthorhombic $CrVO_4$-type structure,[33] whereas nanoribbons synthesized by hydrothermal process present the orthorhombic one. On the other hand, it has been reported that nanofibers of $InVO_4$ can present both structures.[34] These results show the importance of studying the known polymorphs of $InVO_4$.

In an effort to get a better understanding of the behavior of $InVO_4$ at equilibrium and under pressure, we carry out *ab initio* calculations by considering first the well known experimental synthesized phases of this compound to determine the stability of each reported structure: $InVO_4$-I, -III, and -V phases were studied. A complete description of the stable phases is presented in conjunction with the experimental data from literature. After, we go further and we put forward other possible high pressure phases for a range of pressure beyond the one reached in the experiments performed by Errandonea *et al.*[25] to determine the transition pressures at ambient temperature and the range of pressure stability of each phase by using the quasiharmonic approximation. We also report the evolution of phonon frequencies for the most stable polymorphs as well as the phonon spectrum and phonon density of states (PDOS) of each phase, which in turns will help us to determine the stabil-

ity of each phase. In an effort to complement our study, we performed the band structure calculations for the most representative phases of $InVO_4$.

The paper is organized as follows: In the next section, we give a detailed description of the computational procedure. The description of the structure of the experimentally known polymorphs of $InVO_4$ is presented in Sec. 3.1, while the phase transitions driven by pressure are on Sec. 3.2. The study of vibrational and electronic properties of $InVO_4$ are shown in Sec. 3.3 and 3.4, respectively. Finally, the summary and conclusions are given in Sec. 4.

2 Computational details

Calculations of the total energy were performed within the framework of the density functional theory (DFT) and the projector-augmented wave (PAW)[35,36] method as implemented in the Vienna *ab initio* simulation package (VASP).[37–40] A plane-wave energy cutoff of 520 eV was used to ensure a high precision in our calculations. The exchange-correlation energy was described within the generalized gradient approximation (GGA) in the AM05[41–43] formulation.

The Monkhorst-Pack scheme was employed to discretize the Brillouin-zone (BZ) integrations[44] with meshes 3×3×3, 4×3×3, 4×4×2, 4×4×4, and 4×4×2, which correspond to sets of 10, 8, 4, 16, and 8, special k-points in the irreducible BZ for the monoclinic α-$MnMoO_4$-type structure, orthorhombic $CrVO_4$-type structure, the tetragonal scheelite, and the monoclinics wolframite, raspite and $AgMnO_4$-type structures, respectively. For the other phases considered in the high-pressure regime, we use the most suitable mesh for each case. In the relaxed equilibrium configuration, the forces are less than 2 meV/Å per atom in each of the Cartesian directions. This high degree of convergence is required for the calculations of vibrational properties using the direct force constant approach.[45] The partial phonon density of states (PDOS), has been obtained from the calculation of the phonon in the whole BZ at several pressures wih a supercell 2×2×2 times the conventional unit cell. Temperature

effects and zero-point energy have been included within the quasiharmonic approximation[46] through the calculation of the vibrational free energy. The phase transitions at 300 K were obtained analyzing the Gibbs free energy for the phases under study. For the electronic structure the optimized crystal structures were used with a larger set of k-points.

3 Results and Discussion

3.1 Structure of experimentally known polymorphs of $InVO_4$

According to the literature, $InVO_4$ has been successfully synthesized and characterized in three different polymorphs, the monoclinic α-$MnMoO_4$-type $InVO_4$-I,[27,28] the orthorhombic $CrVO_4$-type structure $InVO_4$-III,[24,25] and most recently the wolframite $InVO_4$-V[25] (SG $P2/c$, No. 13, $Z = 2$). While phases I and III crystallize at ambient pressure, phase V was recently identified under pressure.[25] Also, lately *ab initio* calculations were used to study phases III and V.[29] In order to determine the crystal structure and the relative stability of these phases at ambient and high pressure, we carry out the calculations simulations of these phases at different volumes.

The equilibrium volume and unit-cell parameters were calculated by minimizing the crystal total energy for different volumes allowing to relax the internal atomic positions and lattice parameters. The volume-energy data were fitted with a third-order Birch-Murnaghan equation of state (EOS).[47] As is shown in Fig. 2 the lowest energy structure of $InVO_4$ belongs to the $CrVO_4$-type (III) phase followed by the α-$MnMoO_4$-type structure (I) and wolframite (V). Table 1 presents the optimized structural parameters obtained from our calculations, the theoretical results from Mondal *et al.*[29] and the experimental values published in the literature[25,27–29] for comparison. For each phase, the pressure at which the values have been taken is indicated. As expected from a GGA exchange correlation functional, there is a small overestimation of the calculated equilibrium volume with respect to experimental values. In the present case there is a good agreement with a difference of less than 1.5% in the lattice

Table 1: Structural parameters and bulk properties of experimentally known polymorphs of $InVO_4$ at ambient conditions and high pressures. Where a, b, and c are the lattice parameters, V_0 the volume at ambient pressure, B the bulk modulus, and B_0' the pressure derivative of bulk modulus.

	I - α-$MnMoO_4$-type			III - $CrVO_4$-type			V - wolframite			V - $CuWO_4$-type	
	DFT[a]	Exp.[28]	Exp.[27]	DFT[a]	DFT[29]	Exp.[25]	DFT[a]	DFT[29]	Exp.[25]	DFT[a]	Exp.[25]
P (GPa)	atm.	atm.	atm.	atm.	atm.	0.8	8.5	6.0	8.2	8.57	8.2
a (Å)	10.3516	10.271	10.49	5.7547	5.816	5.738	4.7009	4.776	4.714	4.6996	4.714
b (Å)	9.4700	9.403	9.39	8.6168	8.739	8.492	5.5197	5.588	5.459	4.8840	5.459
c (Å)	7.0863	7.038	7.12	6.6751	6.775	6.582	4.8849	4.958	4.903	5.5220	4.903
α (deg.)										90.021	90.2
β (deg.)	104.81	105.08	105.1				92.62	92.89	93.8	90.030	93.8
γ (deg.)										92.588	90.2
Z	8	8	8	4	4	4	2	2	2	2	2
V_0 (Å^3)	671.6	656.3	677.4	331.0	344.37	320.72	126.62	132.17	125.89	126.62	125.89
B_0 (GPa)	120.9			71.0	76.47	69	166.1	183.0	168	166.1	168
B_0'	4.52			4.0	3.0	4.0	4.26	6.0	4.0	4.26	4.0

[a] This work.

parameters with respect to experimental values. Note that the corresponding difference between the results from Mondal *et al.*[29] and the experimental data from Ref. 25 is of the order of 3%, which represents a difference in the equilibrium volume of ≈7.4%. Also, our results, of bulk modulus (B_0) and bulk pressure derivative (B_0'), are in better agreement than those from Mondal *et al.*[29] with respect to the experimental results from Ref. 25. For phase V, the experimental parameters were obtained above 8 GPa since the ambient pressure values are unknown due to the mixture of phases III and V observed once pressure is released from 23.9 GPa. In the next section we will deal with the stability of these phases under pressure.

Reports related to the $InVO_4$-I phase are limited to the work performed by Touboul *et al.*[20,26] and Roncaglia *et al.*[27] This phase has not attracted much attention, due to its low stability. However, it is well known that $InVO_4$-I resembles the structure of $CrVO_4$-I[15] and α-MnMoO4.[48] Therefore, a good description of this phase is needed, furthermore it could help to understand α-MnMoO4 compound and other molibdates with the same structure.[49] The $InVO_4$-I phase has eight f.u. in the unit cell. In this structure there are two nonequivalent positions for In and V and five oxygen positions (Table 2), which leads to several different

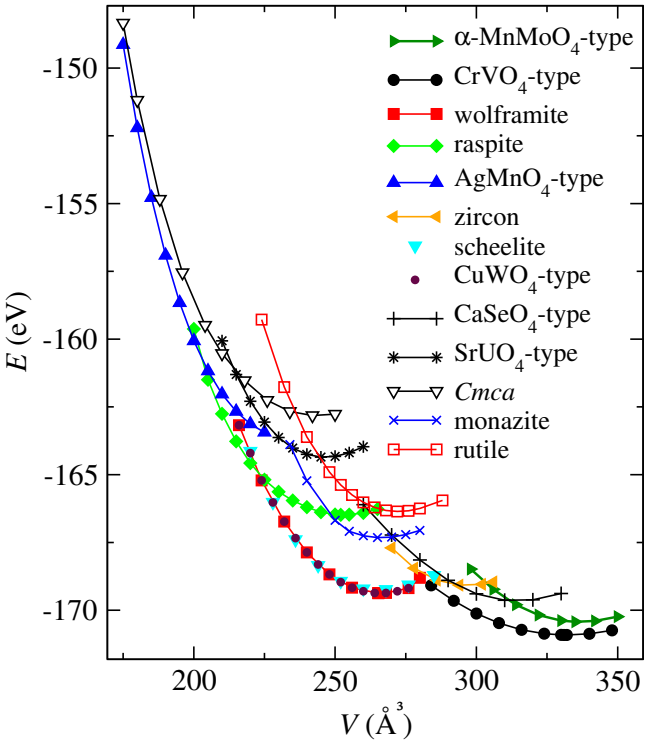

Figure 2: Calculated total energy-volume curves for the studied polymorphs of $InVO_4$.

In-O and V-O bond distances, as can be appreciated in Table 3. The values for In-O (V-O) range from 2.092 (1.671) to 2.267 (1.854) Å, in good agreement with experimental results.[28] In this structure, In and V atoms are surrounded by six and four oxygen atoms, respectively, to form the irregular InO_6 octahedra and VO_4 tetrahedra (Figure 1 a). The four InO_6 units share edges along y and z directions to form In_4O_{16} clusters which share corners with sixteen VO_4 tetrahedras in such a way that layers of In_4O_{16} clusters are formed separated by VO_4 units in the $(20\bar{1})$ plane. The VO_4 units do not share corners with each other, but are connected to the corners of each InO_6 octahedra. We have to mention that the formation of these clusters was not observed in the other phases studied in this work.

Phase III ($CrVO_4$-type) is the most studied phase of $InVO_4$. We just mention that the structure consist of edge-sharing InO_6 octahedra along the c direction, the chains are linked together with VO_4 tetrahedra (Figure 1-a). The tetrahedra and octahedra are more regular than in phase I as can be inferred from the In-O an V-O distances displayed in Table 3. The

Table 2: Wyckoff positions of the experimentally known polymorphs of $InVO_4$ for values of Table 1.

I - α-$MnMoO_4$-type

		DFT			Exp.[28]		
Atom	WP	x	y	z	x	y	z
In_1	$4h$	0	0.1870	0.5	0	0.1875	0.5
In_2	$4i$	0.7892	0	0.1317	0.7907	0	0.1313
V_1	$4g$	0	0.2520	0	0	0.2563	0
V_2	$4i$	0.2737	0	0.4061	0.2737	0	0.402
O_1	$4i$	0.1410	0	0.5394	0.141	0.5	0.541
O_2	$4i$	0.7915	0	0.8374	0.789	0	0.831
O_3	$8j$	0.6324	0.1496	0.1074	0.636	0.153	0.107
O_4	$8j$	0.0481	0.1553	0.8127	0.044	0.161	0.808
O_5	$8j$	0.1393	0.3512	0.5252	0.136	0.350	0.522

III - $CrVO_4$-type

		DFT			DFT[29]			Exp.[25]		
Atom	WP	x	y	z	x	y	z	x	y	z
In	$4a$	0	0	0	0	0	0	0	0	0
V	$4c$	0	0.3581	0.25	0	0.358	0.25	0	0.3617	0.25
O_1	$8g$	0.2575	0.4730	0.25	0.256	0.473	0.25	0.2568	0.4831	0.25
O_2	$8f$	0	0.7543	0.9536	0	0.753	0.953	0	0.7492	0.9573

V - wolframite

		DFT			DFT[29]			Exp.[25]		
Atom	WP	x	y	z	x	y	z	x	y	z
In	$2f$	0.5	0.7040	0.25	0.5	0.704	0.25	0.5	0.711	0.25
V	$2e$	0	0.1814	0.25	0	0.181	0.25	0	0.159	0.25
O_1	$4g$	0.2128	0.9086	0.4574	0.21	0.91	0.46	0.214	0.861	0.492
O_2	$4g$	0.2499	0.3834	0.3885	0.248	0.382	0.386	0.241	0.407	0.399

V - $CuWO_4$-type

		DFT			Exp.[25]		
Atom	WP	x	y	z	x	y	z
In	$2i$	0.4999	0.7498	0.2964	0.5	0.711	0.25
V	$2i$	0.0004	0.7501	0.8188	0	0.159	0.25
O_1	$2i$	0.7871	0.5429	0.0915	0.214	0.861	0.491
O_2	$2i$	0.2127	0.9569	0.0916	0.786	0.861	0.492
O_3	$2i$	0.7501	0.6117	0.6168	0.242	0.407	0.399
O_4	$2i$	0.2500	0.8884	0.6168	0.758	0.407	0.101

apical distances of the InO_6 polyhedra are 2.1392 ($\times$2) Å and the equatorial are 2.1877 ($\times$4) Å. In this structure the VO_4 tetrahedra are not linked to one another. The In and V atoms

Table 3: Interatomic bond distances, In-O and V-O for the experimental known polymorphs of $InVO_4$. The experimental data were taken from Refs. 28 and 25.

	In-O (Å)			V-O (Å)	
	DFT	Exp.		DFT	Exp.
I - α-$MnMoO_4$-type					
In_1-O_1(×2)	2.2667	2.25	V_1-O_3(×2)	1.6714	1.64
In_1-O_4(×2)	2.1645	2.11	V_1-O_4(×2)	1.7848	1.78
In_1-O_5(×2)	2.0969	2.05	V_2-O_1(×1)	1.8544	1.87
In_2-O_1(×1)	2.2571	2.23	V_2-O_2(×1)	1.6856	1.59
In_2-O_2(×1)	2.0917	2.11	V_2-O_5(×2)	1.6763	1.69
In_2-O_3(×2)	2.1276	2.12	⟨In-O⟩	1.7256	1.71
In_2-O_4(×2)	2.1947	2.23			
⟨In-O⟩	2.1708	2.155			
III - $CrVO_4$-type					
In-O_2 (×2)	2.1392	2.1483	V-O_2 (×2)	1.6690	1.6579
In-O_1 (×4)	2.1877	2.1623	V-O_1 (×2)	1.7824	1.7983
⟨In-O⟩	2.1755	2.1588	⟨V-O⟩	1.7257	1.7281
III - $CrVO_4$-type[29]					
In-O_2 (×2)	2.22		V-O_2 (×2)	1.68	
In-O_1 (×4)	2.18		V-O_1 (×2)	1.79	
⟨In-O⟩	2.193		⟨V-O⟩	1.735	
V - wolframite					
In-O_1 (×2)	2.0610	2.0268	V-O_1 (×2)	1.7346	1.6730
In-O_2 (×2)	2.1316	2.1397	V-O_1 (×2)	2.0501	2.2166
In-O_2 (×2)	2.2459	2.2101	V-O_2 (×2)	1.8498	1.8861
⟨In-O⟩	2.1462	2.1255	⟨V-O⟩	1.8782	1.9252
V - wolframite[29]					
In-O_1 (×2)	2.11		V-O_1 (×2)	1.75	
In-O_2 (×2)	2.18		V-O_1 (×2)	2.08	
In-O_2 (×2)	2.29		V-O_2 (×2)	1.87	
⟨In-O⟩	2.193		⟨V-O⟩	1.90	
V - $CuWO_4$-type					
In-O_1 (×1)	2.0605		V-O_1 (×1)	1.7340	
In-O_2 (×1)	2.0607		V-O_2 (×1)	1.7351	
In-O_3 (×1)	2.1313		V-O_3 (×1)	1.8492	
In-O_4 (×1)	2.1319		V-O_4 (×1)	1.8506	
In-O_5 (×1)	2.2445		V-O_5 (×1)	2.0480	
In-O_6 (×1)	2.2453		V-O_6 (×1)	2.0511	
⟨In-O⟩	2.1457		⟨V-O⟩	1.8780	

occupy $4a$ and $4c$ positions, respectively, while there are two nonequivalent oxygen atoms in $8g$ and $8f$ positions, see Table 2. As can be seen from Tables 1 to 3 our results are in good agreement with the experimental data reported in Refs. 24 and 25.

The structure of wolframite-type phase (phase V) was widely studied for other compounds that crystallizes in this structure at ambient pressure, such as ABO_4 [A = Mg, Mn, Fe, Co, Ni, B = Mo, W].[1,50–54] Since the experimental data are reported above 8 GPa, our theoretical description of this phase will be done for the structure at 8.5 GPa. At this pressure there are remarkable differences between this phase and the others previously described. From bond distances in Table 3, it can be deduced that polyhedra InO_6 and VO_6, Fig. 1 (c), are more irregular than in phase III. The structure consist of alternating InO_6 and VO_6 octahedral units that share edges, forming zigzag chains building a close-packed structure.[51] These alternating chains are the reason of the highest bulk modulus of wolframite in comparison with phases I and III. In this structure, the VO_6 octahedra are less compressible than the InO_6 polyhedra.[1] This topic will treated in more detail in the next section.

In order to correlate our results with the experimental ones,[25] we used the coordinates of the reported triclinic $P\bar{1}$ structure, which could be described as a $CuWO_4$-type structure,[55] to calculate the stability of this phase against the wolframite. As seen in Fig. 2 wolframite and $CuWO_4$-type structure are energetically competitive, as a mater of fact it seems that $CuWO_4$-type structure is a distortion of the wolframite one. According to Table 1 to 3 this distortion is small, so small that the difference in the results for phase transitions and phonons are almost negligible, as we will see in the next sections.

3.2 Phase transitions

To the best of our knowledge there are very few studies about the stability of $InVO_4$ under extreme conditions of temperature[24] and pressure.[25,29] The X-ray diffraction pattern of $InVO_4$ in the $CrVO_4$-type structure was reported from ambient temperature to 1023 K.[24] No phase transition in this range of temperature was reported, only a smooth increase in

the unit-cell parameters and a significantly higher conductivity above 723 K were observed. On the other hand, according to the high pressure studies from Ref. 25 the $InVO_4$ undergoes a phase transition at 7 GPa from the $CrVO_4$-type structure to the novel polymorph wolframite, which has been designed as phase V of this compound. This phase transition was accompanied by a volume reduction of 14%. Another phase was also observed among III an V. This phase IV cannot be well described in the experiments performed in Ref. 25 because this phase appears as a minority phase in the X-ray patterns in a small pressure range coexisting with phases III and V.

On the other hand, first-principles calculations were used to study the phase transition from $CrVO_4$-type structure to wolframite.[29] Where a phase transition pressure of 5.6 GPa was reported. In their work Mondal *et al.*[29] reported the pressure evolution of lattice parameters, volume and interatomic bond distances for both phases up to a pressure of 14 GPa.

Regarding to the high pressure behavior of other ABO_4 compounds with $CrVO_4$-type structure, it has been reported that $TiPO_4$ and $InPO_4$ follow the phase transition sequence $CrVO_4$-type $\rightarrow$ zircon $\rightarrow$ scheelite $\rightarrow$ wolframite.[30] The first two transitions were also observed in $TiSiO_4$.[56] Besides, $CaSO_4$ undergoes the next phase transitions: $CrVO_4$-type $\rightarrow$ monazite $\rightarrow$ barite $\rightarrow$ scheelite.[57] While $CaSeO_4$, which crystallizes in an orthorhombic structure with space group very close to the $CrVO_4$-type structure (SG: $Cmca$, No. 64, $Z = 4$), experiments the phase transition sequence $Cmca$ $\rightarrow$ scheelite $\rightarrow$ $AgMnO_4$-type structure.[58] Much less studies have been devoted to study $FeVO_4$ and $CrVO_4$ under pressure.[59,60]

Going beyond the pressures range achieved in the experiments conducted by Errandonea *et al.*,[25] we analyze the high pressure behavior of $InVO_4$ and we consider several possible structures in addition to the known polymorphs reported in the literature. To make the selection of candidates phases we take into consideration the north-east trend followed by other compounds in the Bastide's diagram[1] and previous studies performed in ABO_4 compounds.[6,30,56–60] Among the selected structures are the zircon (SG: $I4_1/amd$, No. 141, $Z = 4$), which is the structure of other vanadates such as $HoVO_4$[61] and $CeVO_4$[11] and, the

scheelite (SG: $I4_1/a$, No. 88, $Z = 4$),[62] which has been reported as a high pressure phase of several vanadates[63] and some compounds that crystallizes in the $CrVO_4$-structure[30,56,57] and in the $Cmca$-type structure.[58]

We have also considered the monazite phase (SG: $P2_1/n$, No. 14, $Z = 4$), this structure occurs frequently among ABO_4 compounds.[14] In particular, this structure is a prototype of high pressure phase of $CrVO_4$-type compounds[6] and has been reported as a high-pressure phase of $PrVO_4$,[64] $CaSO_4$,[57] and $CaSeO_4$.[58] Other phases studied such as raspite (S.G.: $P2_1/a$, No. 14, Z=4) and $AgMnO_4$-type (SG: $P2_1/n$, No. 14, $Z = 4$) were found as a post-scheelite phase of $CaSO_4$,[65] $CaSeO_4$,[58] and $SrCrO_4$.[66] Some other post-scheelite[30] phase were considered as the $SrUO_4$-type (S.G.: $Pbcm$, No. 57, Z= 4) and the distorted rutile phase. The orthorhombic rutile (SG: $Cmmm$, No. 65, $Z = 2$), is a prototype of high pressure phase for $CrVO_4$-type compounds.[6] Two different structures with $Cmca$ space group (No. 64) were also included in our study, one corresponds to the polymorphous reported of $CaSeO_4$ with $Z = 4$,[58] and the other one with 8 f.u. in the unit cell corresponds to the high-pressure phase reported for some AWO_4 compounds.[1] To compare our result with the experimental data, we take into account a triclinic $CuWO_4$-type structure (SG: $P\bar{1}$, No. 2, $Z = 2$).[55] For completeness, we also include the study of the possible decomposition of $InVO_4$ under pressure to form InO + VO_3, in order to found if this matches with the experimental data of phase IV.

The calculated energy-volume curves for the mentioned polymorphs of $InVO_4$ are illustrated in Fig. 2. The relative stability and coexistence pressures of these phases can be extracted by the common-tangent construction.[67] The pressure-enthalpy diagram for the considered structures shows that, besides the known polymorphs of $InVO_4$, only the raspite, $AgMnO_4$-type, and the $CuWO_4$-type are competitive in the high-pressure range. Hence, we only calculate the Gibbs energy for these structures. We have to remember that the calculation of Gibbs free energy by the procedure described in Section 2 is computationally expensive, reason for which we only get the Gibbs free energy for the most representative

phases. Figure 3 shows the pressure evolution of the Gibbs energy difference, ΔG, for the most representative phases at 300 K.

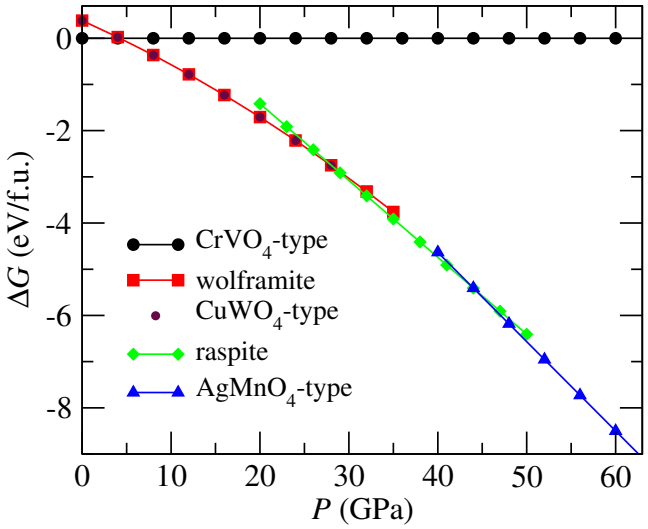

Figure 3: Pressure dependence of Gibbs free energy (at 300 K) for the most stable phases of $InVO_4$.

According to our calculations, the $CrVO_4$-type structure is stable up to 4.4 GPa. For this phase there is a good agreement with the experimental data for the pressure evolution of volume and lattice parameters as is shown in Fig. 4 and 5, respectively. We can see from Fig. 5 that lattice parameter b is more compressible than c and a. This arise from the fact that the InO_6 unit rotates around the y axis as pressure increases because the apical interatomic bond distance of InO_6 polyhedra (In-O_2 in Fig. 6) is less compressible than equatorial ones (In-O_1); this promotes a shortening in the lattice parameter b. This behavior, also observed in $CaSO_4$,[57] differs from that observed in $TiSiO_4$,[56] $InPO_4$, and $TiPO_4$[30] where the apical In-O_2 bond distance remains almost constant under pressure. On the other hand, since V-O_2 distances are oriented in the c direction, the compression of this axis is due to the reduction of the equatorial bond distances of InO_6, as V-O_2 remain almost constant under pressure.

At 4.4 GPa the $CrVO_4$-type structure undergoes a first order phase transition as can be seen in Fig. 3. Experimentally, prior to the transition to wolframite-type, a transition to a phase IV was observed. However it was not possible to give a description of this struc-

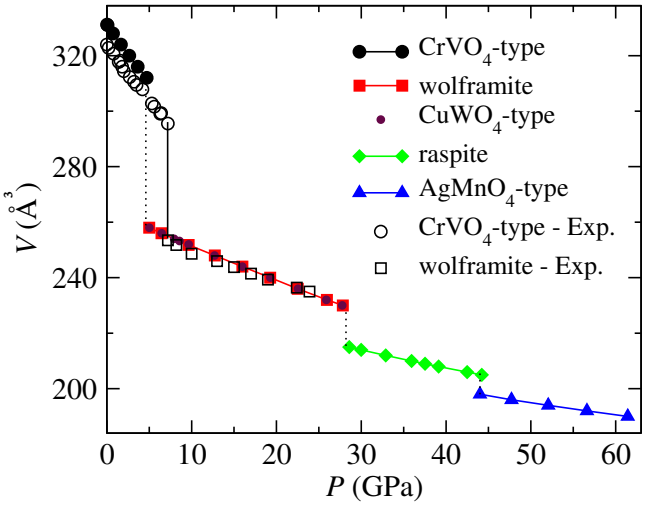

Figure 4: Volume curves as function of pressure for the most stable polymorphs of $InVO_4$. The experimental data was taken from Ref. 25. Vertical doted (continuous) lines show the path followed in the phase transitions obtained from DFT calculations (experiments).

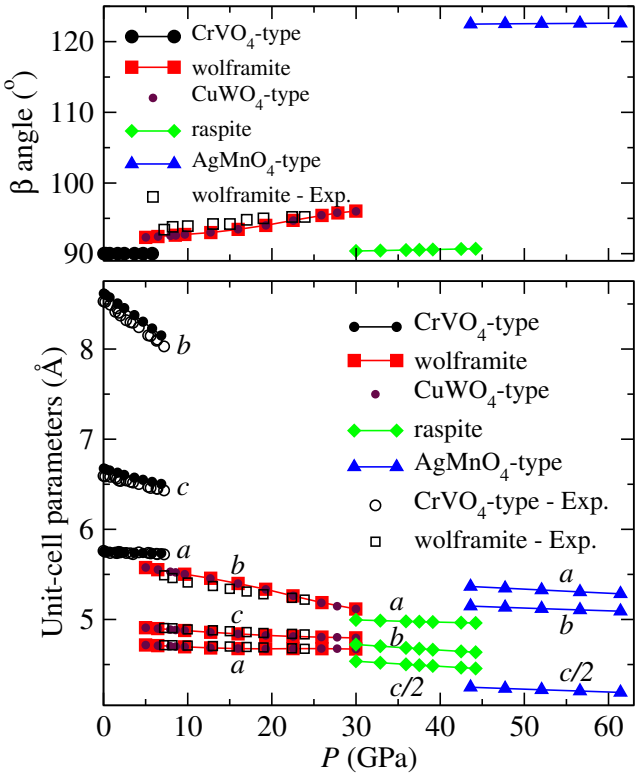

Figure 5: Pressure dependence of β angle and lattice parameters for the studied polymorphs of $InVO_4$. The experimental data was taken from Ref. 25.

ture.[25] According to Fig. 2 scheelite-type and $CuWO_4$-type structure are competitive with wolframite-type. In order to find the phase IV we compare the simulated X-ray diffraction

patterns of these structures with the experimental ones reported in Ref. 25, however the patterns of scheelite-type structure do not fit with the experimental one. We also compare the simulated X-ray patterns of the products of decomposition of $InVO_4$ and we did not find an agreement with the diffraction patterns of $InO+VO_3$. Hence, the description of phase IV will be left for a future work. According to our results, the wolframite and $CuWO_4$-type structure has almost the same energy, where the $CuWO_4$-type could be considered as a distortion of the wolframite; hence, the crystallographic parameters from the $CuWO_4$-type structure are almost the same as the wolframite, see Table 1 to 3 and Figures 2 to 6. We will see in the next section that phonons from wolframite and the $CuWO_4$-type structure are very similar.

In the transition from $CrVO_4$-type to wolframite-type $InVO_4$ experiments a large volume reduction of 16.8%, in good agreement with the experimental value, see Fig. 4. This change is associated with a change in the coordination of the polyhedron around V, from VO_4 to VO_6. Figure 5 shows that lattice parameters and β angle obtained from calculations in very good agreement with the experimental results. From this picture it can be seen that lattice parameter b is much more compressible than a and c, which almost remains constant. Bond lengths In-O in this phase behave in a similar way as in $CrVO_4$-type. The apical bond distance (In-O_2 in the middle zone of Fig. 6 (a)) is less compressible than the other In-O bond distances. It is important to mention the changes in the trend of wolframite interatomic bond distances around 14 GPa (see Fig. 6). One V-O_1 and the In-O bond distances change they trends and the InO_6 polyhedra becomes more irregular. These changes are not reflected in the lattice parameters but they play an important role in the vibrational properties that will be discussed in Sec. 3.3.

According to Fig. 3 the wolframite phase is stable up to 28.1 GPa, then $InVO_4$ presents a transition to the monoclinic raspite structure (phase VI). This transition is accompanied of a volume reduction of 6.5 %. Experiments on $InVO_4$ were conducted only up to 24 GPa,[25] reason for which this phase transition was not observed. The lattice parameters of raspite for

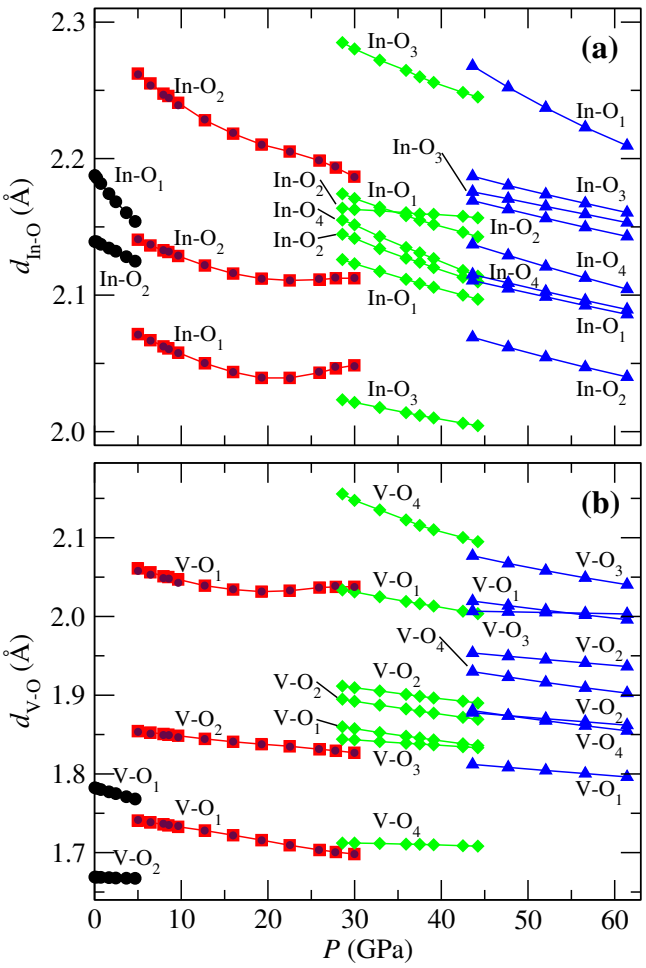

Figure 6: Pressure dependence of interatomic bond distances (a) In-O and (b) V-O. Black circles, red squares, green diamonds, and blue triangles correspond to $CrVO_4$-type, wolframite, raspite, and $AgMnO_4$-type structures, respectively.

a volume of 212 Å^3 and a pressure of 32.9 GPa are a = 4.9869 Å, b = 4.7032 Å, c = 9.0390 Å, and β = 90.51°. In this structure all the non equivalent atoms are located in the 4e WP: In (0.5334, 0.2408, 0.6182), V (0.03432, 0.2457, 0.8893), O1 (0.2290, 0.9886, 0.03418), O2 (0.2089, 0.003844, 0.5248), O3 (0.3813, 0.2795, 0.8235), and O4 (0.09154, 0.8490, 0.7789). We found from the EOS a bulk modulus of B_0 = 112.72 GPa with V_0 = 252.77 Å^3 and B_0' = 4.25. From lattice parameters and β angle presented in Fig.5 we observe that this phase resembles a distorted tetragonal structure, it consists of alternating zig-zag chains of InO_7 polyhedra in the z direction linked by VO_7 units. InO_7 polyhedra share edges in the zig-zag chains running perpendicular to plane [010], whereas they just share the corners in the z

Table 4: Calculated Raman and infrared phonon frequencies for phases III (at ambient pressure) and V (at 6.44 GPa) of $InVO_4$ in the Γ point. Frequencies ω are in cm^{-1} and $d\omega/dP$ in cm^{-1}/GPa.

	$InVO_4$-III - $CrVO_4$						$InVO_4$-V - wolframite						$InVO_4$-V - $CuWO_4$		
	DFT			Exp.[25]			DFT			Exp.[25]			DFT		
	ω	$d\omega/dp$	γ	ω	$d\omega/dp$		ω	$d\omega/dp$	γ	ω	$d\omega/dp$		ω	$d\omega/dp$	γ
$T(B_{3g})$	128.36	1.47	0.37	135	2.1	B_g	108.15	0.13	0.24	109	1.8	A_g	108.15	0.12	0.22
$T(B_{1g})$	153.78	-2.38	-0.60	191	0.7	A_g	124.43	0.05	0.08	118	1.9	A_g	124.39	0.05	0.08
$T(A_g)$	193.24	0.27	0.07	218	4.5	B_g	139.17	0.75	1.04	145	2.0	A_g	139.24	0.76	1.05
$R(B_{1g})$	208.32	4.93	1.24	252	3.6	B_g	189.11	1.42	1.44	149	-0.1	A_g	189.01	1.43	1.45
$R(B_{2g})$	237.68	3.88	0.98	342	0.4	B_g	214.33	1.74	1.55	204	1.5	A_g	214.26	1.77	1.57
$\nu_2(A_g)$	334.48	0.37	0.09	348	5.6	A_g	241.95	-0.52	-0.43	223	2.2	A_g	242.18	-0.58	-0.48
$R(B_{3g})$	352.16	5.01	1.27	377	1.9	B_g	289.68	1.06	0.71	241	0.0	A_g	289.61	1.07	0.72
$\nu_4(B_{1g})$	361.53	1.38	0.35	389	4.4	A_g	304.06	0.74	0.47	251	1.1	A_g	304.26	0.72	0.46
$\nu_2(B_{2g})$	370.74	4.64	1.17	390	1.4	A_g	340.75	1.23	0.70	319	1.2	A_g	340.99	1.13	0.65
$\nu_4(A_g)$	380.68	1.33	0.34	456	5.2	B_g	379.81	1.95	1.00	336	2.4	A_g	379.61	1.95	0.99
$\nu_4(B_{3g})$	422.85	6.14	1.55	637	7.2	A_g	420.14	1.90	0.88	347	1.6	A_g	420.11	1.88	0.87
$\nu_3(B_{1g})$	657.99	7.59	1.92	755	5.7	B_g	440.53	3.87	1.67	378	1.9	A_g	440.39	3.87	1.67
$\nu_3(A_g)$	752.49	6.36	1.61	847	4.2	B_g	499.37	3.37	1.30	433	2.0	A_g	499.34	3.39	1.30
$\nu_1(A_g)$	920.05	1.33	0.34	914	1.3	A_g	520.75	2.32	0.86	531	1.8	A_g	520.79	2.29	0.85
$\nu_3(B_{3g})$	925.12	2.34	0.59	918	2.1	B_g	679.84	5.04	1.41	684	5.1	A_g	679.70	5.13	1.44
						A_g	712.73	4.22	1.14	723	3.8	A_g	712.93	4.20	1.13
						B_g	740.12	5.15	1.33	758	5.2	A_g	740.05	5.20	1.34
						A_g	835.15	4.62	1.07	850	4.4	A_g	836.02	4.62	1.06
$T(B_{1u})$	102.64	0.14	0.04			B_u	72.15	-7.61	-11.97			A_u	72.49	-7.98	-14.00
$T(B_{3u})$	150.91	-2.09	-0.53			A_u	175.83	-0.08	-0.09			A_u	176.03	-0.17	-0.20
$T(B_{1u})$	152.31	0.85	0.22			B_u	200.95	-0.05	-0.05			A_u	201.02	-0.08	-0.07
$T(B_{2u})$	214.39	0.20	0.05			B_u	267.83	-0.43	-0.32			A_u	267.80	-0.45	-0.33
$R(B_{3u})$	253.72	4.42	1.13			A_u	293.65	-0.34	-0.23			A_u	293.68	-0.38	-0.25
$T(B_{2u})$	253.85	1.21	0.31			B_u	316.80	2.58	1.55			A_u	316.73	2.58	1.55
$\nu_4(B_{3u})$	328.31	2.06	0.52			A_u	361.33	-0.60	-0.33			A_u	361.33	-0.61	-0.33
$R(B_{1u})$	346.36	6.73	1.71			B_u	366.10	1.75	0.93			A_u	365.90	1.74	0.92
$\nu_2(B_{2u})$	358.37	-0.03	-0.01			A_u	456.57	3.04	1.28			A_u	456.67	3.01	1.26
$\nu_4(B_{2u})$	396.86	3.69	0.94			B_u	497.00	3.84	1.48			A_u	496.97	3.85	1.48
$\nu_4(B_{1u})$	423.21	4.95	1.26			B_u	531.83	4.27	1.53			A_u	531.79	4.31	1.54
$\nu_3(B_{3u})$	681.81	7.29	1.86			A_u	544.80	3.75	1.32			A_u	544.90	3.74	1.31
$\nu_1(B_{2u})$	758.20	6.59	1.68			A_u	610.39	4.98	1.56			A_u	610.49	5.04	1.57
$\nu_3(B_{1u})$	893.20	1.72	0.44			B_u	697.88	5.14	1.41			A_u	698.08	5.27	1.44
$\nu_3(B_{2u})$	936.59	0.94	0.24			A_u	761.40	3.91	1.00			A_u	760.86	3.95	1.00

direction. The same behavior was observed for VO_7 polyhedra. Figure 6 shows that both In-O and V-O interatomic bond distances have similar compressibility, except for one V-O_4

Table 5: Calculated Raman frequencies for raspite and $AgMnO_4$-type structures of $InVO_4$ at 30 and 47.7 GPa in the Γ point. Frequencies ω are in cm^{-1} and $d\omega/dP$ in cm^{-1}/GPa.

	$InVO_4$-VI - raspite				$InVO_4$-VII - $AgMnO_4$		
	ω	$d\omega/dp$	γ		ω	$d\omega/dp$	γ
B_g	149.38	0.02	0.03	B_g	141.70	0.26	0.60
A_g	154.28	0.55	0.88	A_g	153.75	0.51	1.15
B_g	160.19	0.89	1.41	B_g	172.96	0.43	0.98
A_g	160.95	0.68	1.08	A_g	189.07	0.60	1.36
B_g	175.50	0.51	0.81	A_g	199.15	0.36	0.82
A_g	188.77	0.64	1.01	B_g	224.80	0.69	1.56
A_g	196.31	1.51	2.39	A_g	241.85	0.98	2.23
A_g	230.57	1.69	2.67	B_g	308.66	0.83	1.88
B_g	268.70	1.31	2.08	A_g	312.23	0.61	1.40
B_g	272.34	1.50	2.37	A_g	332.98	1.34	3.06
A_g	287.58	1.36	2.15	B_g	349.16	1.05	2.40
A_g	306.89	1.82	2.87	A_g	362.50	1.29	2.95
B_g	313.30	0.81	1.28	A_g	383.38	1.31	2.98
B_g	317.27	1.79	2.83	B_g	388.12	1.35	3.08
A_g	366.91	1.39	2.20	A_g	430.25	1.32	3.00
A_g	376.11	1.58	2.51	B_g	434.29	1.33	3.04
B_g	382.82	1.48	2.34	A_g	465.14	1.11	2.53
B_g	395.89	0.97	1.54	B_g	471.55	1.36	3.09
A_g	399.66	0.63	1.00	B_g	474.75	1.50	3.42
B_g	404.40	1.80	2.84	A_g	485.99	1.78	4.05
A_g	448.47	1.51	2.39	B_g	502.54	1.45	3.31
B_g	472.82	1.74	2.75	B_g	530.49	1.65	3.76
A_g	481.82	1.56	2.46	A_g	555.38	1.93	4.40
B_g	503.14	1.76	2.78	A_g	563.88	2.49	5.68
A_g	519.02	1.80	2.85	B_g	568.75	1.94	4.43
B_g	549.77	2.26	3.58	B_g	593.57	1.60	3.64
B_g	630.57	2.60	4.12	B_g	636.40	1.94	4.41
A_g	638.81	2.73	4.33	A_g	640.11	1.84	4.19
B_g	683.74	2.26	3.58	A_g	695.62	2.25	5.12
A_g	729.24	2.45	3.87	B_g	719.83	2.02	4.61
B_g	729.71	2.45	3.87	B_g	724.57	2.46	5.62
A_g	750.96	2.51	3.98	A_g	738.48	2.32	5.28
A_g	784.38	1.91	3.02	B_g	773.84	2.43	5.53
A_g	817.94	2.78	4.41	A_g	778.88	2.33	5.30
B_g	821.21	3.05	4.83	B_g	825.34	2.41	5.50
B_g	902.50	2.00	3.17	A_g	863.67	2.39	5.46

and one In-O_2 bond distances that are almost constants in all the range of pressure stability.

As pressure increases, respite becomes unstable and $InVO_4$ undergoes a phase transition

Table 6: Calculated infrared frequencies for raspite and $AgMnO_4$-type structures of $InVO_4$ at 30 and 47.7 GPa in the Γ point. Frequencies ω are in cm^{-1} and $d\omega/dP$ in cm^{-1}/GPa.

	$InVO_4$-VI - raspite				$InVO_4$-VII - $AgMnO_4$		
	ω	$d\omega/dp$	γ		ω	$d\omega/dp$	γ
B_u	80.13	0.57	0.91	A_u	159.25	0.67	1.53
A_u	106.41	0.84	1.34	A_u	193.84	0.58	1.33
A_u	119.36	0.82	1.29	B_u	195.88	0.61	1.40
B_u	176.56	1.14	1.81	B_u	249.45	1.16	2.66
A_u	183.84	0.69	1.09	A_u	253.19	0.94	2.16
B_u	225.00	0.56	0.89	A_u	278.71	1.05	2.40
A_u	243.98	1.27	2.01	B_u	289.05	1.21	2.77
A_u	260.53	2.42	3.83	A_u	333.88	0.98	2.24
B_u	289.55	1.65	2.62	A_u	361.07	1.13	2.59
A_u	289.91	1.05	1.67	B_u	366.60	1.62	3.70
B_u	312.00	1.59	2.51	A_u	387.75	0.89	2.05
A_u	330.01	1.38	2.19	B_u	393.32	1.40	3.21
B_u	339.55	2.37	3.75	A_u	424.11	1.71	3.90
A_u	357.23	1.94	3.08	B_u	435.82	1.01	2.32
B_u	379.75	0.88	1.40	A_u	451.90	2.28	5.22
A_u	401.66	1.68	2.66	B_u	453.84	1.59	3.63
B_u	420.91	2.45	3.89	B_u	464.04	1.91	4.37
A_u	443.83	1.88	2.98	A_u	476.15	1.29	2.94
B_u	455.67	2.06	3.26	B_u	505.51	1.40	3.20
A_u	491.46	2.09	3.31	A_u	508.74	2.16	4.93
B_u	493.27	2.02	3.20	B_u	560.65	1.58	3.60
B_u	522.22	2.75	4.35	B_u	601.75	1.81	4.15
A_u	526.72	2.15	3.41	A_u	623.33	1.71	3.91
B_u	548.07	1.93	3.05	B_u	629.23	1.96	4.48
A_u	555.61	2.01	3.19	A_u	650.58	2.29	5.23
A_u	605.22	2.39	3.78	B_u	659.22	2.11	4.82
B_u	606.18	2.22	3.51	A_u	680.57	1.91	4.36
B_u	676.83	2.50	3.96	B_u	724.84	2.36	5.38
A_u	701.39	2.73	4.33	A_u	732.64	2.38	5.43
B_u	765.13	2.73	4.33	B_u	776.58	2.19	4.99
A_u	790.99	2.16	3.43	A_u	795.32	2.39	5.47
A_u	840.92	2.64	4.18	A_u	813.90	2.23	5.10
B_u	850.70	2.45	3.87	B_u	815.64	2.60	5.93

to the $AgMnO_4$-type structure at 44 GPa (phase VII). As can be seen in Fig. 4 there is just a small volume reduction in the transition from raspite to the $AgMnO_4$-type structure, ΔV = -3.5 %. At 52 GPa the lattice parameters of this phase are a = 5.3266 Å, b = 5.1199

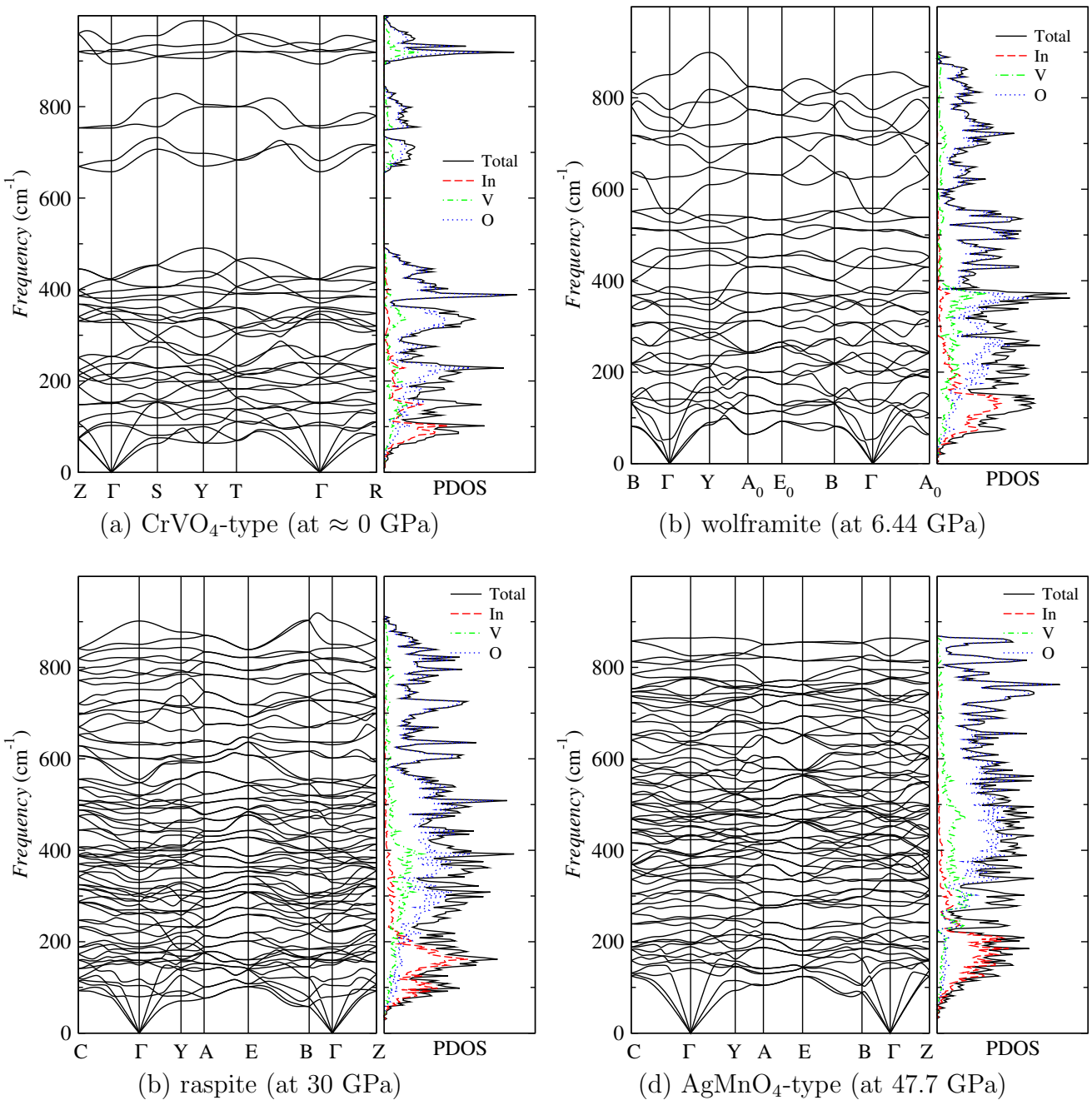

(a) $CrVO_4$-type (at ≈ 0 GPa)

(b) wolframite (at 6.44 GPa)

(b) raspite (at 30 GPa)

(d) $AgMnO_4$-type (at 47.7 GPa)

Figure 7: Phonon spectrum and PDOS of $InVO_4$.

Å, $c = 8.4399$ Å, and $\beta = 122.56$ °, the volume 194 Å^3. The Figure 5 shows that although raspite and $AgMnO_4$-type phases belongs to the same SG, they have marked differences in the lattice parameters, however they have almost the same compressibility. This is also reflected in the change of interatomic bond distances as function of pressure. Like in raspite-type, in this phase the In, V, and O atoms are located in the 4*e* WP as follow: In (0.3725,

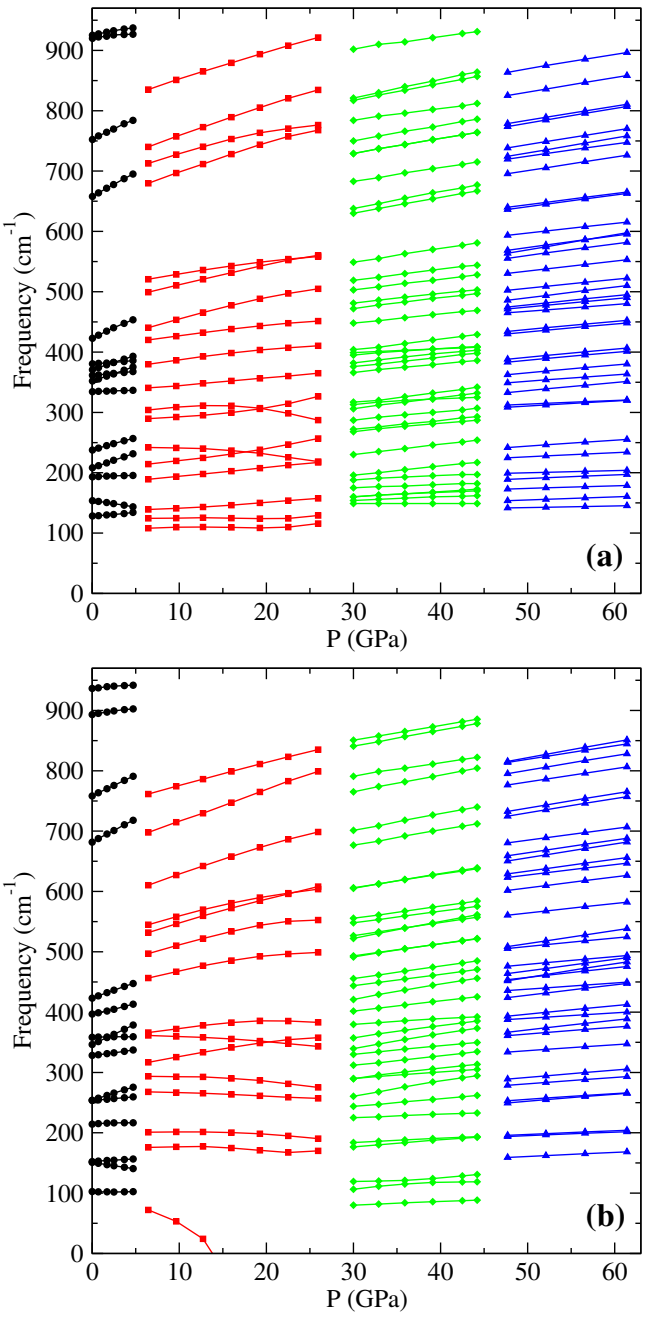

Figure 8: Pressure dependence of (a) Raman and (b) IR frequencies of $InVO_4$. Black circles, red squares, green diamonds, and blue triangles corresponds to $CrVO_4$-type, wolframite, raspite and $AgMnO_4$-type structures, respectively.

0.06524, 0.12899), V (0.9727, 0.005625, 0.6706), O1 (0.7477, 0.9612, 0.4191), O2 (0.9497, 0.3533, 0.5960), O3 (0.3198, 0.2113, 0.8709), and O4 (0.7676, 0.2088, 0.7487). This phase is formed by InO_8 and VO_8 units that shares edges and corners. The InO_8 polyhedra forms

layers that lay in the *bc* plane, separated by layers formed by VO_8 polyhedra. We found that $InVO_4$ is stable in this phase up to 62 GPa, which is the highest pressure reached in this study.

3.3 Vibrational properties

Nowadays the lattice vibration studies, through the analysis of Raman (R) and Infrared (IR) spectra from experimental as well as theoretical methods, have become fundamental tools to understand the behavior of materials at ambient conditions and under extreme conditions of temperature and pressure.[46,67] In particular, these studies help to determine and realize whether a phase transition takes place. In many cases the experimental and theoretical approximations are conjugated with great success to study AVO_4 compounds, see for example references 11, 68, 64, 69 and references there in; whereas in other circumstances the theoretical results serve as a guide for future experimental and theoretical studies.[30,58] In this section we analyze the lattice dynamics of $InVO_4$ in the phases III, V, raspite (VI) and $AgMnO_4$-type (VII) by means of the calculated phonon frequencies at Γ point for each phase, their pressure dependence, and Grüneisen parameters as well as their dispersion relation along the Brillouin zone and partial density of states (PDOS).

The calculated and experimental R and IR frequencies at Γ point for the studied phases appear in Table 4 to 6, the pressure coefficients ($d\omega/dP$,) and Grüneisen parameters [γ = -$\partial(\ln\,\omega)/\partial(\ln\,V)$] were also included. The phonon relation of dispersion and the PDOS are displayed in Fig. 7. The vibrational modes of $InVO_4$ can be classified as internal or external modes of the VO_4 unit. The external modes correspond either to a pure translation (T) or to a pure rotation (R) of the VO_4 unit. Whereas the internal modes of the VO_4 tetrahedra are ν_1 (symmetric stretching), ν_2 (symmetric bending), ν_3 (asymmetric stretching), and ν_4 (asymmetric bending).[30] The T modes are usually the lowest in frequency, the ν_x modes are the highest in frequency, and the frequencies of the R modes are between those of the T and ν_x modes.

According to the group theory analysis, the $Cmcm$ space group of $CrVO_4$-type structure has the following representation at Γ point: $\Gamma = 5A_g + 4B_{1g} + 6B_{1u} + 3A_u + 2B_{2g} + 7B_{2u} + 4B_{3g} + 5B_{3u}$. Where there are three acoustic modes: B_{1u}, B_{2u}, and B_{3u}, three silent modes A_u, 15 infrared active modes: $5B_{1u}$, $6B_{2u}$, and $4B_{3u}$, and 15 Raman active modes: $5A_g$, $4B_{1g}$, $2B_{2g}$, and $4B_{3g}$.[30] As can be seen in Table 4 this phase presents two T and one ν_2 phonons that are characterized by a decrease of the vibrational frequency with pressure, i.e. negative pressure coefficients and Grüneisen parameters, the Raman mode B_{1g} (153.78 cm^{-1}) and two IR modes: B_{3u} (150.91 cm^{-1}) and B_{2u} (358.37 cm^{-1}). The softening of this B_{1g} Raman (B_{3u} IR) mode was also observed in $CaSO_4$[57] ($InPO_4$),[30] and could be related with the instability of the $CrVO_4$-type structure under pressure. The pressure evolution of Raman and IR modes of the studied phases is displayed in Fig. 8 (a) and (b), respectively. The phonon dispersion for $CrVO_4$, Fig. 7 (a), shows no imaginary frequency. We also realized simulation of phonon dispersions up to ≈7 GPa and no significant changes were observed. As seen on the PDOS, phonons above 600 cm^{-1} belong to internal ν_x modes, i.e. there are only contributions from V and O. The frequencies of the external modes are located below 255 cm^{-1}, and the intermediate is occupied by external (R) and internal (ν) modes.

For wolframite the group theory predicts the following Γ phonon modes: $\Gamma = 8A_g + 10B_g + 8A_u + 10B_u$. Here $2B_u$ and one A_u infrared modes are acoustic, 18 are Raman ($8A_g + 10B_g$) and 15 are infrared ($7A_u + 9B_u$). The group theory predicts the same modes for $CuWO_4$-type structure at Γ point. According to Table 4 both phases wolframite and $CuWO_4$-type structure presents almost the same phonon frequencies at 6.44 GPa. Besaides, we observed that phonon spectrum for both phases are very similar, reason for which we only include the spectrum from wolframite.

Figure 8 (a) shows that the slope of some Raman modes of wolframite starts to change around 16 GPa, so that we calculated the pressure coefficients and Grüneisen parameters from Table 4 by considering just the frequencies from 6 to 14 GPa which correspond to the linear trend for wolframite phase. This change in the frequencies of wolframite is due to a

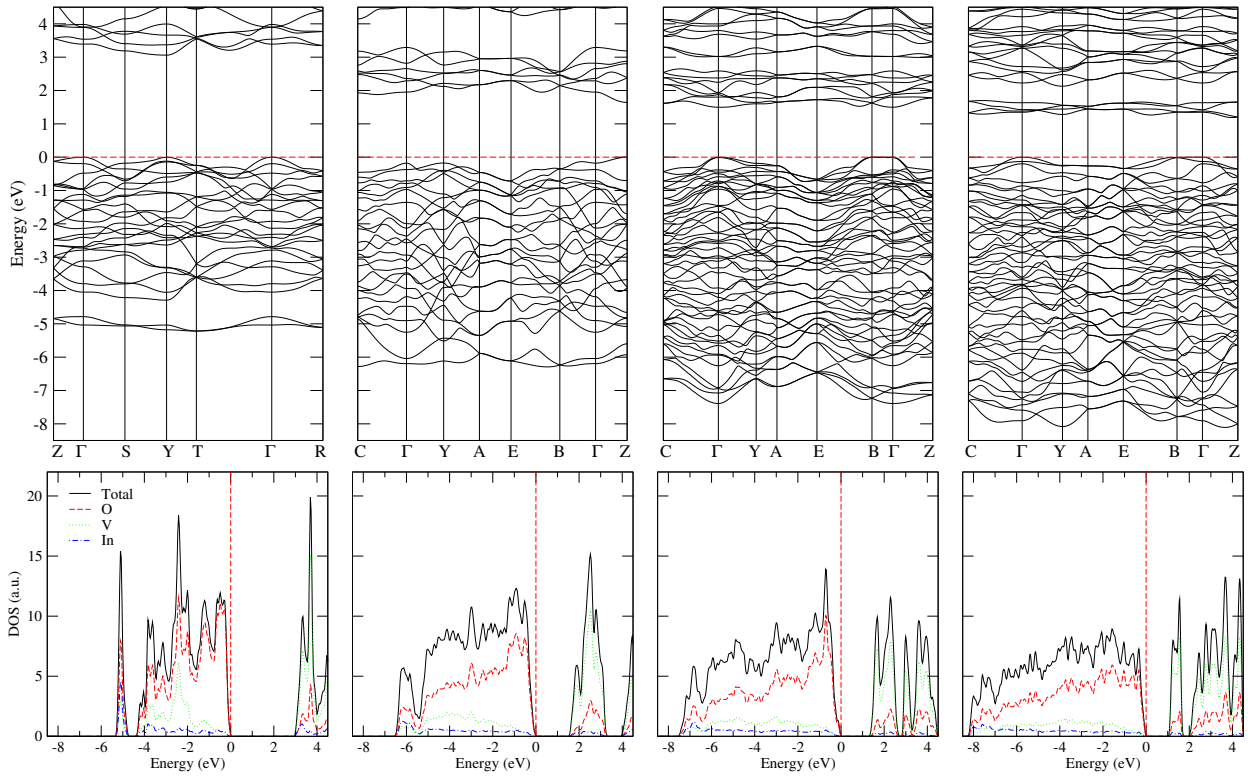

(a) $CrVO_4$-type at ≈ 0 GPa | (b) wolframite at 8 GPa | (c) raspite at 30 GPa | (d) $AgMnO_4$-type at 47.7 GPa

Figure 9: (Color online) Band structure and partial density of states (DOS) of the most stable polymorphs of $InVO_4$.

shift in the slope of the In-O_x and V-O_1 interatomic bond distances as pressure increases, see Fig. 6. Having in mind this, we see that wolframite presents several R and IR phonon modes with negative pressure coefficients. It is noteworthy that B_u IR mode softens completely around 14 GPa, to our knowledge this behavior was not observed previously in other $CrVO_4$-type compounds. However, it has been also reported that this mode softens in the wolframite high-pressure phase of $InPO_4$ and $TiPO_4$,[30] and in other compounds that crystallizes at ambient pressure in the wolframite structure such as $MgWO_4$[50] and $InTaO_4$.[70] The Figure 7 (b) shows the phonon spectra and PDOS of wolframite at ≈9 GPa. At this pressure the first acoustic IR B_u phonon mode softens in two zones of the BZ: C-Γ and Γ-Z; below 4 GPa other acoustic B_u IR mode softens completely between Γ and Z special points. On the other hand, above 14 GPa the B_u has imaginary frequency in Γ point but also in other special

and intermediate points of the BZ. In another way, the phonon spectrum does not present imaginary frequencies once In is eight-fold coordinated above 34 GPa. We also performed the calculation of the phonon spectrum with other bigger supercells in order to eliminate possible errors from the supercell method, but we always found the same results. We see from Fig. 7 (b) that in this phase of $InVO_4$ it is not depicted the phonon gap observed in the wolframite of $InPO_4$ and $TiPO_4$.[30]

Group theory predicts that monoclinic raspite and $AgMnO_4$-type structures have the following vibrational representation for R and IR phonon modes at the Γ point: $\Gamma = 18B_g + 18A_g + 16B_u + 17A_u$, i.e. 36 R and 33 IR active modes. As we can see from Tables 5 and 6 and from Fig. 8 that all Raman and IR phonon modes shift to higher frequencies upon compression, i.e. the pressure coefficients and Grüneisen parameters are positive. The phonon spectrum for these phases no present imaginary frequencies in all the range of pressure studied. For these phases there is not a gap in the PDOS like happens in other compounds with these structures such as $CaSeO_4$.[58] In these phases there is not a clear separation of the internal and external modes due to the high coordination of In and V, also because their interatomic bond distances are different between each other, see the contributions of In and V to the PDOS of Fig. 7.

3.4 Electronic properties

Density functional theory has been used with success to describe the electronic structure of ABO_4 compounds.[11,52,71] In particular, optical-absorption measurements in conjunction with *ab initio* calculations were used to study the electronic structure of zircon-type vanadates as function of pressure.[11,72]

In this section we describe the results about the electronic structure of the most stable polymorphs of $InVO_4$ and the pressure evolution of the energy gap. Figure 9 shows the band structure and the partial density of states of (a) $CrVO_4$-type, (b) wolframite, (c) raspite, and (d) $AgMnO_4$-type phases at the respective pressure. Whereas Fig. 10 shows the pressure

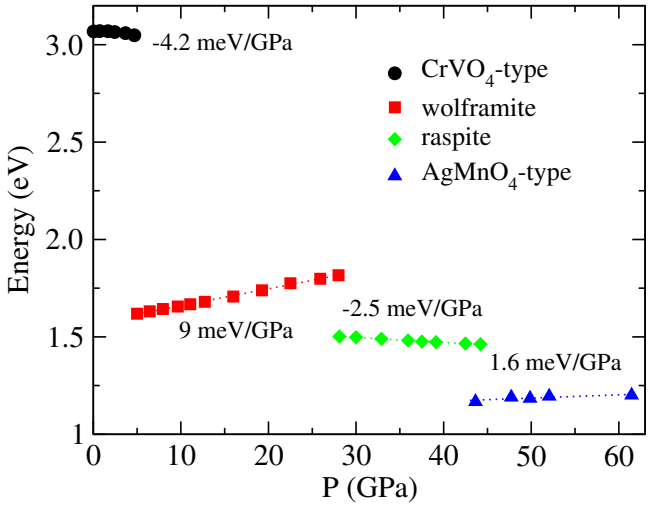

Figure 10: (Color online) Pressure evolution of gap energy of $InVO_4$.

evolution of the energy gap of $InVO_4$.

According to our calculations of band structure, Fig. 9 (a), the phase III of $InVO_4$ is an indirect band-gap material (top of valence band at Γ and bottom of conduction band at Y). Where the top of the valence band consists mainly of O $2p$ states. The bottom of the conduction band is dominated by V $3d$ states with a not negligible contribution of O $2p$ and In $5s$ states. Similar results were obtained in Refs. 29 and 73. For this phase an indirect band gap of 3.06 eV was obtained in excellent agreement with the experimental value of 3.2 eV reported by Enache *et al.*[22] Whereas the predicted theoretical values of 3.24 and 4.02 eV were reported in Refs. 73 and 29, respectively.

As pressure increases the band-gap in phase III is reduced with a pressure coefficient of -4.2 meV/GPa, as seen on Fig. 10. At the phase transition from $CrVO_4$-type structure to wolframite we observed a collapse of the band gap which becomes close to 1.6 eV. In this phase we observed that the top of the valence band and the bottom of conduction band are located at Z point. Again, the orbital contribution to the top of the valence band and the bottom of the conduction band is similar than in the low-pressure phase but the conduction band are also populated with small contributions from O $2s$ and In $5p$. The band gap collapse is consistent with the observation made in the study performed by Errandonea

et al. in reference 25. On the other hand, the theoretical results from Ref. 29 show that wolframite phase is an indirect band-gap material with the top of the valence band at Z and the bottom of the conduction band at Γ. Contrary to the band-gap behavior of $CrVO_4$-type structure under pressure, the band gap of wolframite increases with pressure with a pressure coefficient of 9 meV/GPa. Similar values were observed in the high pressure studies of other wolframites such as $MgWO_4$, $ZnWO_4$ and $CdWO_4$.[52]

As seen in Fig. 9 (c) raspite phase has a direct band-gap at Γ point. While $AgMnO_4$-type behave like a indirect band-gap material with the top of the valence band at Γ and the bottom of the conduction band at Z point. In these phases the top of the valence band is almost all populated by O $2p$ states, whereas the bottom of the conduction band is mainly occupied by V $3d$ states. In these phases it is produced additional reductions of the band gap becoming the band gap of $AgMnO_4$-type phase 1.2 eV at 60 GPa. Consequently, the band gap of $InVO_4$ changes from 3.06 eV at ambient pressure to 1.2 eV at 60 GPa, behaving the material as a narrow-gap semiconductor. Such a large change of the electronic band gap has only been observed in $PbCrO_4$ for ABO_4 oxides.[74]

4 Summary and Conclusions

We presented a first principles study of structural, electronic and vibrational properties of $InVO_4$ from ambient pressure to 62 GPa. The quasi-harmonic approximation has been used to obtain the Gibbs free energy and determine the phase transitions at ambient temperature. Where a good agreement between our theoretical results and the reported experimental data was obtained. In our study we found that wolframite presents o drastic change in the interatomic bond distances in order to increase the coordination of In at elevated pressures, which has an important effect in the Raman and infrared phonon frequencies at Γ point, but also in the branches of the phonon spectrum in other points of the Brillouin zone. It has been observed that the characteristic acoustic B_u infrared phonon mode of wolframite,

the phonon mode that has negative pressure coefficient and Grüneisen parameter, softens completely around 14 GPa. Which is related with the instability of the wolframite phase as pressure increases. Besides, in our study two new high pressure phases were observed above 28 GPa, being the raspite and $AgMnO_4$-type structure. As is known the last one was observed as post-scheelite phase in $CaSeO_4$ and as high-pressure phase of $CaSO_4$.

It has been proposed that pressure could induce the metallization of orthovanadates at relative low pressure (11 GPa)[75] however our calculations show that $InVO_4$ does not become metallic up to 60 GPa.

The information of transition pressure and volume reduction involved in the phase transition sequence observed in $InVO_4$ in this study from phase III ($CrVO_4$-) to VII ($AgMnO_4$-type structure) can be summarized as follows:

$$\text{III} \xrightarrow[\Delta V=-16.8\ \%]{P_T=4.4\ \text{GPa}} \text{V} \xrightarrow[-6.5]{28.1} \text{VI} \xrightarrow[-3.5]{44} \text{VII}$$

Author Information

Corresponding Author

*E-mail: sinlopez@uacam.mx

Author Contributions

The manuscript was written through contributions of all authors. All authors have given approval to the final version of the manuscript.

Notes

The authors declare no competing financial interests.

Acknowledgement

This work has been done under partial financial support from Spanish MINECO under projects MAT2013-46649-C4-1/3-P, MAT2015-71070-REDC, and MAT2016-75586-C4-1/3-

P. S.M.L. thanks CONACYT from Mexico for financial support through the program "Cátedras para Jóvenes Investigadores". We thank the computer time provided by the RES (Red Española de Supercomputación) and the MALTA cluster.

References

(1) Errandonea, D.; Manjón, F. J. Pressure effects on the structural and electronic properties of ABX_4 scintillating crystals. *Prog. Mater. Sci.* **2008**, *53*, 711–773.

(2) Rapaport, A.; David, V.; Bass, M.; Deka, C.; Boatner, L. Optical spectroscopy of erbium-doped lutetium orthophosphate. *J. Luminescence* **1999**, *85*, 155–161.

(3) Rapaport, A.; Moteau, O.; Bass, M.; Boatner, L. A.; Deka, C. Optical spectroscopy and lasing properties of neodymium-doped lutetium orthophosphate. *J. Opt. Soc. Am. B* **1999**, *16*, 911–916.

(4) Lempicki, A.; Berman, E.; Wojtowicz, A.; Balcerzyk, M.; Boatner, L. Cerium-doped orthophosphates: new promising scintillators. *Nuclear Science, IEEE Transactions on* **1993**, *40*, 384–387.

(5) Allison, S. W.; Boatner, L. A.; Gillies, G. T. Characterization of high-temperature thermographic phosphors: spectral properties of $LuPO_4$:Dy(1%),Eu(2%). *Appl. Opt.* **1995**, *34*, 5624–5627.

(6) Baran, E. J. Materials belonging to the $CrVO_4$ structure type: preparation, crystal chemistry and physicochemical properties. *J. Mater. Sci.* **1998**, *33*, 2479–2497.

(7) Ai, Z.; Zhang, L.; Lee, S. Efficient Visible Light Photocatalytic Oxidation of NO on Aerosol Flow-Synthesized Nanocrystalline $InVO_4$ Hollow Microspheres. *J. Phys. Chem. C* **2010**, *114*, 18594–18600.

(8) Lin, H.-Y.; Chen, Y.-F.; Chen, Y.-W. Water splitting reaction on $NiO/InVO_4$ under visible light irradiation. *Inter. J. Hydrogen Energy* **2007**, *32*, 86–92.

(9) Dennis P. Butcher, J.; Gewirth, A. A. Photoelectrochemical Response of $TlVO_4$ and $InVO_4$: $TlVO_4$ Composite. *Chem. Mater.* **2010**, *22*, 2555–2562.

(10) Zou, Z.; Ye, J.; Sayama, K.; Arakawa, H. Direct splitting of water under visible light irradiation with an oxide semiconductor photocatalyst. *Nature* **2001**, *414*, 625–627.

(11) Panchal, V.; López-Moreno, S.; Santamaría-Pérez, D.; Errandonea, D.; Manjón, F. J.; Rodríguez-Hernandez, P.; Muñoz, A.; Achary, S. N.; Tyagi, A. K. Zircon to monazite phase transition in $CeVO_4$: X-ray diffraction and Raman-scattering measurements. *Phys. Rev. B* **2011**, *84*, 024111.

(12) Errandonea, D.; Lacomba-Perales, R.; Ruiz-Fuertes, J.; Segura, A.; Achary, S. N.; Tyagi, A. K. High-pressure structural investigation of several zircon-type orthovanadates. *Phys. Rev. B* **2009**, *79*, 184104.

(13) Tomeno, I.; Sato, N.; Sato, Y.; Oka, K.; Tsunoda, Y. Neutron scattering study of acoustic phonon softening in $BiVO_4$. *Phys. Rev. B* **2011**, *84*, 014302.

(14) Clavier, N.; Podor, R.; Dacheux, N. Crystal chemistry of the monazite structure. *J. European Ceramic Soc.* **2011**, *31*, 941–976.

(15) Touboul, M.; Melghit, K. Synthesis by Chimie douce and properties of chromium (III) vanadates(V). *J. Mater. Chem.* **1995**, *5*, 147–150.

(16) Tojo, T.; Zhang, Q.; Saito, F. Mechanochemical synthesis of rutile-type $CrMO_4$ (M=V, Sb) and their solid solutions. *J. Solid State Chem.* **2006**, *179*, 433–437.

(17) Oka, Y.; Yao, T.; Yamamoto, N.; Ueda, Y.; Kawasaki, S.; Azuma, M.; Takano, M. Hydrothermal Synthesis, Crystal Structure, and Magnetic Properties of $FeVO_4$-II. *J. Solid State Chem.* **1996**, *123*, 54–59.

(18) Robertson, B.; Kostiner, E. Crystal structure and Mössbauer effect investigation of $FeVO_4$. *J. Solid State Chem.* **1972**, *4*, 29–37.

(19) Muller, J.; Joubert, J. Synthese sous haute pression d'oxygene d'une forme dense ordonne'e de $FeVO_4$ et mise en evidence d'une varie'te'allotropique de structure $CrVO_4$. *J. Solid State Chem.* **1975**, *14*, 8–13.

(20) Touboul, M.; Ingrain, D. Syntheses et propriétés thermiques de $InVO_4$ et $TlVO_4$. *J. Less Common Metals* **1980**, *71*, 55–62.

(21) Baran, E. J.; Escobar, M. E. The vibrational spectra of $InVO_4$ and $TlVO_4$. *Spectrochimica Acta Part A: Molecular Spectroscopy* **1985**, *41*, 415–417.

(22) Enache, C. S.; Lloyd, D.; Damen, M. R.; Schoonman, J.; van de Krol, R. Photoelectrochemical Properties of Thin-Film $InVO_4$ Photoanodes: the Role of Deep Donor States. *J. Phys. Chem. C* **2009**, *113*, 19351–19360.

(23) van de Krol, R.; Ségalini, J.; Enache, C. S. Influence of point defects on the performance of $InVO_4$ photoanodes. *J. Photonics Energy* **2011**, *1*, 016001–016001–10.

(24) Katari, V.; Patwe, S. J.; Achary, S. N.; Tyagi, A. K. High Temperature Structural, Dielectric, and Ion Conduction Properties of Orthorhombic $InVO_4$. *J. Amer. Ceram. Soc.* **2013**, *96*, 166–173.

(25) Errandonea, D.; Gomis, O.; García-Domene, B.; Pellicer-Porres, J.; Katari, V.; Achary, S. N.; Tyagi, A. K.; Popescu, C. New Polymorph of $InVO_4$: A High-Pressure Structure with Six-Coordinated Vanadium. *Inorg. Chem.* **2013**, *52*, 12790–12798.

(26) Touboul, M.; Tolédano, P. Structure du vanadate d'indium: $InVO_4$. *Acta Cryst. B* **1980**, *36*, 240–245.

(27) Roncaglia, D.; Botto, I.; Baran, E. Characterization of a low-temperature form of $InVO_4$. *J. Solid State Chem.* **1986**, *62*, 11–15.

(28) Touboul, M.; Melghit, K.; Bénard, P.; Louër, D. Crystal Structure of a Metastable Form of Indium Orthovanadate, $InVO_4$-I. *J. Solid State Chem.* **1995**, *118*, 93–98.

(29) Mondal, S.; Appalakondaiah, S.; Vaitheeswaran, G. High pressure structural, electronic, and optical properties of polymorphic $InVO_4$ phases. *J. Appl. Phys.* **2016**, *119*, 085702.

(30) López-Moreno, S.; Errandonea, D. *Ab initio* prediction of pressure-induced structural phase transitions of $CrVO_4$-type orthophosphates. *Phys. Rev. B* **2012**, *86*, 104112.

(31) Wang, Y.; Cao, G. Synthesis and electrochemical properties of $InVO_4$ nanotube arrays. *J. Mater. Chem.* **2007**, *17*, 894–899.

(32) Liu, J.; Cao, G.; Yang, Z.; Wang, D.; Dubois, D.; Zhou, X.; Graff, G.; Pederson, L.; Zhang, J.-G. Oriented Nanostructures for Energy Conversion and Storage. *Chem. Sus. Chem.* **2008**, *1*, 676–697.

(33) Yi, X.; Li, J.; Chen, Z.; Tok, A. Single-Crystalline InVO4 Nanotubes by Self-Template-Directed Fabrication. *J. Amer. Ceram. Soc.* **2010**, *93*, 596–600.

(34) Song, L.; Liu, S.; Lu, Q.; Zhao, G. Fabrication and characterization of electrospun orthorhombic $InVO_4$ nanofibers. *Appl. Surf. Sci.* **2012**, *258*, 3789–3794.

(35) Blöchl, P. E. Projector augmented-wave method. *Phys. Rev. B* **1994**, *50*, 17953–17979.

(36) Kresse, G.; Joubert, D. From ultrasoft pseudopotentials to the projector augmented-wave method. *Phys. Rev. B* **1999**, *59*, 1758–1775.

(37) Kresse, G.; Hafner, J. *Ab initio* molecular dynamics for liquid metals. *Phys. Rev. B* **1993**, *47*, 558–561.

(38) Kresse, G.; Hafner, J. *Ab initio* molecular-dynamics simulation of the liquid-metal-amorphous-semiconductor transition in germanium. *Phys. Rev. B* **1994**, *49*, 14251–14269.

(39) Kresse, G.; Furthmüller, J. Efficiency of ab-initio total energy calculations for metals and semiconductors using a plane-wave basis set. *Comput. Mat. Sci.* **1996**, *6*, 15.

(40) Kresse, G.; Furthmüller, J. Efficient iterative schemes for *ab initio* total-energy calculations using a plane-wave basis set. *Phys. Rev. B* **1996**, *54*, 11169–11186.

(41) Armiento, R.; Mattsson, A. E. Functional designed to include surface effects in self-consistent density functional theory. *Phys. Rev. B* **2005**, *72*, 085108.

(42) Mattsson, A. E.; Armiento, R. Implementing and testing the AM05 spin density functional. *Phys. Rev. B* **2009**, *79*, 155101.

(43) Mattsson, A. E.; Armiento, R.; Paier, J.; Kresse, G.; Wills, J. M.; Mattsson, T. R. The AM05 density functional applied to solids. *J. Chem. Phys.* **2008**, *128*, 084714.

(44) Monkhorst, H. J.; Pack, J. D. Special points for Brillouin-zone integrations. *Phys. Rev. B* **1976**, *13*, 5188–5192.

(45) Parlinski, K. Computer Code PHONON. See: http://wolf.ifj.edu.pl/phonon.

(46) Baroni, S.; de Gironcoli, S.; Dal Corso, A.; Giannozzi, P. Phonons and related crystal properties from density-functional perturbation theory. *Rev. Mod. Phys.* **2001**, *73*, 515–562.

(47) Birch, F. Finite Elastic Strain of Cubic Crystals. *Phys. Rev.* **1947**, *71*, 809–824.

(48) Abrahams, S. C.; Reddy, J. M. Crystal Structure of the TransitionMetal Molybdates. I. Paramagnetic AlphaMnMoO$_4$. *J. Chem. Phys.* **1965**, *43*, 2533–2543.

(49) Sleight, A. W.; Chamberland, B. L. Transition metal molybdates of the type AMoO$_4$. *Inorg. Chem.* **1968**, *7*, 1672–1675.

(50) Ruiz-Fuertes, J.; López-Moreno, S.; Errandonea, D.; Pellicer-Porres, J.; Lacomba-Perales, R.; Segura, A.; Rodríguez-Hernández, P.; Muñoz, A.; Romero, A. H.; González, J. High-pressure phase transitions and compressibility of wolframite-type tungstates. *J. Appl. Phys.* **2010**, *107*, 083506.

(51) Ruiz-Fuertes, J.; Errandonea, D.; López-Moreno, S.; González, J.; Gomis, O.; Vilaplana, R.; Manjón, F. J.; Muñoz, A.; Rodríguez-Hernández, P.; Friedrich, A.; Tupitsyna, I. A.; Nagornaya, L. L. High-pressure Raman spectroscopy and lattice-dynamics calculations on scintillating $MgWO_4$: Comparison with isomorphic compounds. *Phys. Rev. B* **2011**, *83*, 214112.

(52) Ruiz-Fuertes, J.; López-Moreno, S.; López-Solano, J.; Errandonea, D.; Segura, A.; Lacomba-Perales, R.; Muñoz, A.; Radescu, S.; Rodríguez-Hernández, P.; Gospodinov, M.; Nagornaya, L. L.; Tu, C. Y. Pressure effects on the electronic and optical properties of AWO_4 wolframites (A = Cd, Mg, Mn, and Zn): The distinctive behavior of multiferroic $MnWO_4$. *Phys. Rev. B* **2012**, *86*, 125202.

(53) López-Moreno, S.; Romero, A. H.; Rodríguez-Hernández, P.; Muñoz, A. Ab initio calculations of the wolframite $MnWO_4$ under high pressure. *High Press. Res.* **2009**, *29*, 578–581.

(54) Sleight, A. W. Accurate cell dimensions for ABO_4 molybdates and tungstates. *Acta Cryst. B* **1972**, *28*, 2899–2902.

(55) Ruiz-Fuertes, J.; Errandonea, D.; Lacomba-Perales, R.; Segura, A.; González, J.; Rodríguez, F.; Manjón, F. J.; Ray, S.; Rodríguez-Hernández, P.; Muñoz, A.; Zhu, Z.; Tu, C. Y. High-pressure structural phase transitions in $CuWO_4$. *Phys. Rev. B* **2010**, *81*, 224115.

(56) Gracia, L.; Beltrán, A.; Errandonea, D. Characterization of the TiSiO4 structure and its pressure-induced phase transformations: Density functional theory study. *Phys. Rev. B* **2009**, *80*, 094105.

(57) Gracia, L.; Beltrán, A.; Errandonea, D.; Andrés, J. $CaSO_4$ and Its Pressure-Induced Phase Transitions. A Density Functional Theory Study. *Inorg. Chem.* **2012**, *51*, 1751–1759.

(58) López-Moreno, S.; Errandonea, D.; Rodríguez-Hernández, P.; Muñoz, A. Polymorphs of $CaSeO_4$ under Pressure: A First-Principles Study of Structural, Electronic, and Vibrational Properties. *Inorg. Chem.* **2015**, *54*, 1765–1777.

(59) Young, A. P.; Schwartz, C. M. High pressure forms of $CrVO_4$ and $FeVO_4$. *Acta Cryst.* **1962**, *15*, 1305.

(60) Laves, F.; Young, A. P.; Schwartz, C. M. On the high-pressure form of $FeVO_4$. *Acta Cryst.* **1964**, *17*, 1476–1477.

(61) Garg, A. B.; Errandonea, D.; Rodríguez-Hernández, P.; López-Moreno, S.; Muñoz, A.; Popescu, C. High-pressure structural behaviour of HoVO 4 : combined XRD experiments and abinitio calculations. *J. Phys.: Condens. Matter* **2014**, *26*, 265402.

(62) López-Moreno, S.; Rodríguez-Hernández, P.; Muñoz, A.; Romero, A. H.; Errandonea, D. First-principles calculations of electronic, vibrational, and structural properties of scheelite EuWO4 under pressure. *Phys. Rev. B* **2011**, *84*, 064108.

(63) Panchal, V.; Errandonea, D.; Segura, A.; Rodríguez-Hernández, P.; Muñoz, A.; López-Moreno, S.; Bettinelli, M. The electronic structure of zircon-type orthovanadates: Effects of high-pressure and cation substitution. *J. Appl. Phys.* **2011**, *110*, 043723.

(64) Errandonea, D.; Achary, S. N.; Pellicer-Porres, J.; Tyagi, A. K. Pressure-Induced Transformations in $PrVO_4$ and $SmVO_4$ and Isolation of High-Pressure Metastable Phases. *Inorg. Chem.* **2013**, *52*, 5464–5469.

(65) Crichton, W. A.; Parise, J. B.; Antao, S. M.; Grzechnik, A. Evidence for monazite-, barite-, and $AgMnO_4$ (distorted barite)-type structures of $CaSO_4$ at high pressure and temperature. *Mineral. Mag.* **2005**, *90*, 22–27.

(66) Gleissner, J.; Errandonea, D.; Segura, A.; Pellicer-Porres, J.; Hakeem, M. A.; Proctor, J. E.; Raju, S. V.; Kumar, R. S.; Rodríguez-Hernández, P.; Muñoz, A.; Lopez-

Moreno, S.; Bettinelli, M. Monazite-type $SrCrO_4$ under compression. *Phys. Rev. B* **2016**, *94*, 134108.

(67) Mujica, A.; Rubio, A.; Muñoz, A.; Needs, R. J. High-pressure phases of group-IV, III˘V, and II˘VI compounds. *Rev. Mod. Phys.* **2003**, *75*, 863–912.

(68) Panchal, V.; Manjón, F. J.; Errandonea, D.; Rodriguez-Hernandez, P.; López-Solano, J.; Muñoz, A.; Achary, S. N.; Tyagi, A. K. High-pressure study of $ScVO_4$ by Raman scattering and *ab initio* calculations. *Phys. Rev. B 83*, 064111.

(69) Errandonea, D.; Manjón, F.; Munoz, A.; Rodríguez-Hernández, P.; Panchal, V.; Achary, S.; Tyagi, A. High-pressure polymorphs of TbVO4: A Raman and ab initio study. *J. Alloys Compounds* **2013**, *577*, 327 – 335.

(70) Errandonea, D.; Popescu, C.; Garg, A. B.; Botella, P.; Martinez-García, D.; Pellicer-Porres, J.; Rodríguez-Hernández, P.; Muñoz, A.; Cuenca-Gotor, V.; Sans, J. A. Pressure-induced phase transition and band-gap collapse in the wide-band-gap semiconductor $InTaO_4$. *Phys. Rev. B* **2016**, *93*, 035204.

(71) Lacomba-Perales, R.; Errandonea, D.; Segura, A.; Ruiz-Fuertes, J.; Rodriguez-Hernandez, P.; Radescu, S.; Lopez-Solano, J.; Mujica, A.; Munoz, A. A combined high-pressure experimental and theoretical study of the electronic band-structure of scheelite-type AWO_4 (A=Ca, Sr, Ba, Pb) compounds. *J. Appl. Phys.* **2011**, *110*, 043703.

(72) Paszkowicz, W.; Lopez-Solano, J.; Piszora, P.; Bojanowski, B.; Mujica, A.; Munoz, A.; Cerenius, Y.; Carlson, S.; Dabkowska, H. Equation of state and electronic properties of $EuVO_4$: A high-pressure experimental and computational study. *J. Alloys Comp.* **2015**, *648*, 1005–1016.

(73) Li, G.-L.; Yin, Z. Theoretical insight into the electronic, optical and photocatalytic properties of InMO4 (M = V, Nb, Ta) photocatalysts. *Phys. Chem. Chem. Phys.* **2011**, *13*, 2824–2833.

(74) Errandonea, D.; Bandiello, E.; Segura, A.; Hamlin, J.; Maple, M.; Rodriguez-Hernandez, P.; noz, A. M. Tuning the band gap of PbCrO4 through high-pressure: Evidence of wide-to-narrow semiconductor transitions. *J. Alloys Comp.* **2014**, *587*, 14–20.

(75) Garg, A. B.; Shanavas, K.; Wani, B.; Sharma, S. M. Phase transition and possible metallization in CeVO4 under pressure. *J. Solid State Chem.* **2013**, *203*, 273–280.

Graphical TOC Entry

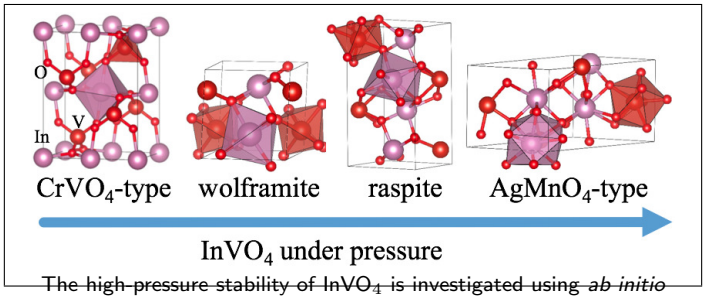

The high-pressure stability of $InVO_4$ is investigated using *ab initio* calculations. Where the phase transitions driven by pressure were determined within the quasiharmonic approximation at 300 K. In our findings two new HP post-wolframite phases were obtained. The equation of state, crystal structure, phonon spectrum and electronic structure were studied for each stable phase as well as their evolution with pressure.